Hot compression deformation behavior and constitutive model of 2050 Al-Li alloy

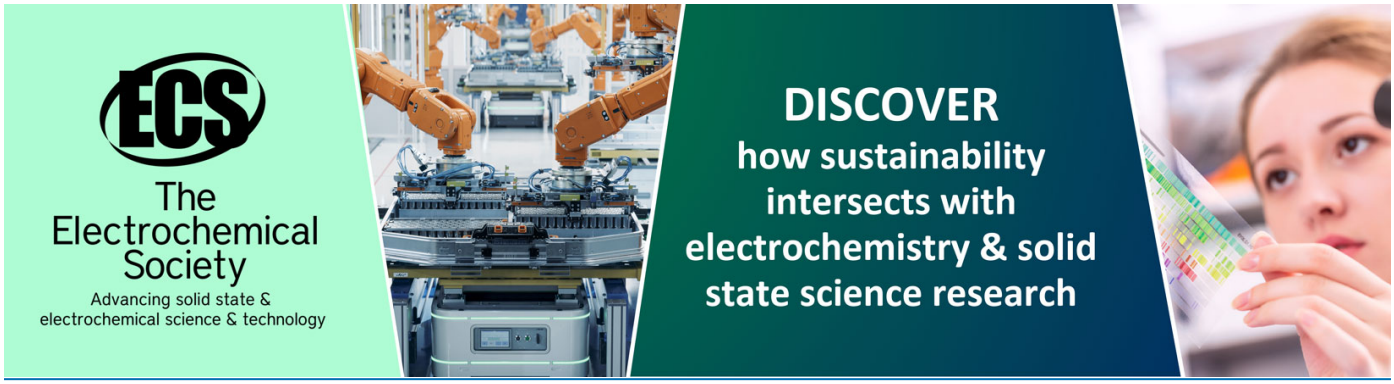

Hot compression deformation behavior and constitutive model of 2050 Al-Li alloy

Lingjiao Wang[1,a], Xiaoqiang Li[1,b*], Weijie Lin[1,c], Dezhi Zhu[1,d], Shengguan Qu[1,e], Xia Huang[2,f], Qijie Feng[3,g]

[1]National engineering research center for near-net-shape for metallic materials, south china university of technology, 510640, Guangzhou, P. R. China

[2]AVIC Manufacturing Technology Institute, Beijing,100024, P. R. China

[3]Institute of nuclear physics and chemistry, Chinese Academy of Engineering Physics, Mianyang,621999, P. R. China

[a]email: wanglj1108@163.com

*Corresponding author: [b]email: Lixq@scut.edu.cn

Abstract: Isothermal compression experiments of 2050 AL-Li alloy were carried out by Gleeble-3800 thermal-mechanical simulator. Hot compression deformation behavior of the alloy under the conditions of deformation temperature of 300~500 ℃ and strain rate of 0.01~10 s^{-1} was studied. The constitutive model of thermal deformation was established. Results indicate that there is an obvious rheological steady state in the isothermal compression process of 2050 aluminum alloy. The microstructure shows that the alloy has recrystallization. 2050 aluminum alloy is a positive strain rate sensitive material. At constant temperature, the steady state flow stress increases with the increase of strain rate. Arrhenius constitutive model can accurately predict the rheological behavior of 2050 aluminum alloy. The average absolute relative error (AARE) of the relative error between the experimental value and the predicted value is 8.59%.

1. Introduction

2XXX series aluminum alloys are widely used in transportation and aerospace industries because of their high strength and low density [1]. As one of the 3rd generation Al-Li alloys, 2050 aluminum alloy has excellent static and fatigue properties [2]. Through forging, rolling and other processes, 2050 aluminum alloy can be processed into components for aircraft wings, fuselage and other parts [3]. Due to the influence of microstructure, deformation temperature, strain rate and stress-strain state of deformation area in the hot working process of Al-Li alloy, improper process may lead to defects such as part cracking.

The constitutive model reflects the coupling relationship between strain stress, strain rate and temperature, so it is an important basis for the formulation and optimization of hot working process. At present, many studies have been carried out on the thermal deformation behavior of aluminum alloys [4,5]. For example, Ning Liu et al. [6] discussed the flow stress characteristics of 2055 aluminum alloy at 480 ℃ ~ 540 ℃, and established the constitutive model of the alloy. Zhenyang Chen et al. [7] established the thermal deformation constitutive model of 2219 aluminum alloy at 330 ℃ ~ 450 ℃. However, the research on the hot deformation behavior of 2050 aluminum alloy is limited. In addition, the establishment of constitutive model in previous studies is based on a narrow temperature range. In

this paper, 2050 aluminum alloy was compressed at high temperature, the high temperature thermal deformation behavior of 2050 aluminum alloy was studied, and the constitutive model of the alloy was established.

2. Experimental materials and methods

The experimental material was 2050 aluminum alloy rolled plate, and its main chemical composition was shown in Table 1. The alloy was processed into a size of Φ 8mm × 12 mm standard hot compression specimen. The thermal compression test was carried out on Gleeble-3800 thermal-mechanical simulator.

Table 1 Chemical composition of as-received 2050 alloy (wt%)

Cu	Li	Mn	Mg	Ti	Fe	Si	Al
3.92	0.98	0.35	0.25	0.03	0.02	0.01	Bal.

According to the deformation temperature and strain rate of 2050 aluminum alloy in actual production, isothermal compression tests were carried out at different temperatures (300, 350, 400, 450 and 500 ℃) and different strain rates (0.01, 0.1, 1 and 10 s^{-1}). The specific process route was shown in Fig. 1. After isothermal compression, the specimens were cut along the center of the compression axis to observe the microstructure of the section. After grinding, polishing and Keller reagent corrosion, the microstructure was characterized by optical microscope.

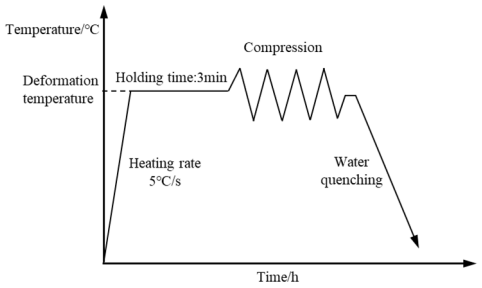

Fig. 1 2050 Al-Li alloy hot compression test procedure.

3. Results and discussion

3.1. True stress - strain curve

Fig. 2 shows the true stress true strain curve of 2050 Al-Li alloy after compression at different deformation temperatures and strain rates. As shown in the Fig. 2a, b, c and d with the increase of true strain, the true stress - strain curves at different deformation temperatures have the same trend. The true stress gradually increases to the peak, then decreases slowly, and finally tends to be stable. This can be attributed to the interaction between work hardening and dynamic softening. At a constant strain rate, the true stress decreases with the increase of temperature. This is because the increase of temperature leads to the increase of atomic kinetic energy and easier diffusion, which is conducive to softening behaviors such as dynamic recovery or dynamic recrystallization. At a constant temperature, the steady flow stress increases with the increase of strain rate, indicating that 2050 Al-Li alloy is a positive strain rate sensitive material.

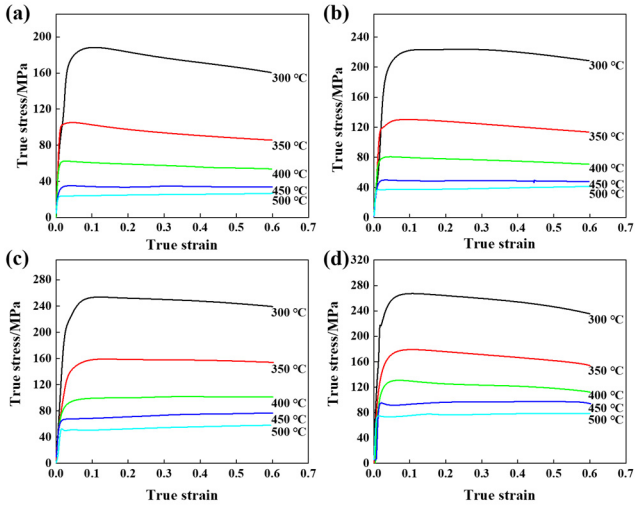

Fig. 2 true stress - strain curve under different strain rates:
(a)$\dot{\varepsilon} = 0.01s^{-1}$; (b)$\dot{\varepsilon} = 0.1s^{-1}$; (c)$\dot{\varepsilon} = 1s^{-1}$; (d)$\dot{\varepsilon} = 10s^{-1}$.

3.2. Isothermal compression microstructure

Fig. 3 shows the microstructure of 2050 aluminum alloy before and after isothermal compression. It can be seen that the obvious fibrous structure is shown in Fig. 3a, which is a typical structure of aluminum alloy after rolling. There are two softening mechanisms in Al-Li alloys: dynamic recovery and dynamic recrystallization [8,9]. At the deformation temperature of 450 ℃ and the strain rate of 1 s^{-1}, equiaxed small particles of dynamic recrystallization appear along the grain boundary (as shown in the circle area of Fig. 3b), which proves that dynamic recrystallization occurs in the deformation process of 2050 aluminum alloy under this process condition. The area of dynamic recrystallization is concentrated near the centerline perpendicular to the compression direction, which may be related to the friction force on the specimen.

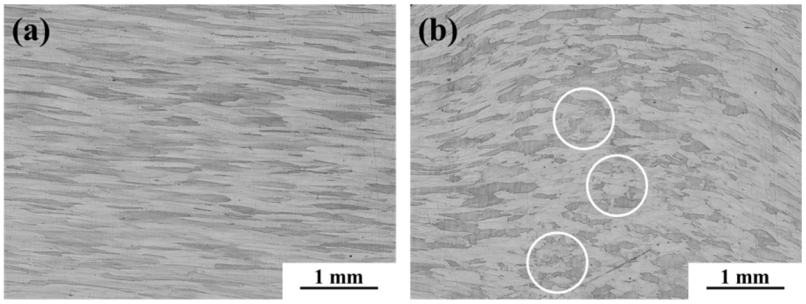

Fig. 3 microstructure of 2050 aluminum alloy before and after isothermal compression: (a) before isothermal compression, (b) after isothermal compression at temperature of 450 ℃ and strain rate of 1 s^{-1}.

3.3. Constitutive model

The flow stress of 2050 aluminum alloy depends on deformation temperature and strain rate. In this paper, Arrhenius constitutive model [10] is used to describe the relationship between the three parameters:

$$\dot{\varepsilon} = Af(\sigma)\, exp(\frac{-Q}{RT}) \quad (1)$$

At low stress levels ($\alpha\sigma < 0.8$) [11] :

$$f(\sigma) = \sigma^{n_1} \quad (2)$$

At high stress level ($\alpha\sigma > 1.2$) [11]:

$$f(\sigma) = exp(\beta\sigma) \quad (3)$$

Throughout the stress range:

$$f(\sigma) = [\sinh(\alpha\sigma)]^n \quad (4)$$

Therefore, under all stress states, Eq.1 can be expressed as:

$$\dot{\varepsilon} = A[\sinh(\alpha\sigma)]^n \, exp(\frac{-Q}{RT}) \quad (5)$$

Where, f(σ) is a function related to the stress level, $\dot{\varepsilon}$ is the strain rate (s^{-1}), σ is the flow stress (MPA), T is the absolute temperature (k), Q is the thermal deformation activation energy ($kJ \cdot mol^{-1}$), and R is the gas constant; Parameter A, n, α, β are constants, where A is the structural influence factor, n is the stress index, and α=β/n. The relationship between flow stress and thermal deformation conditions can be expressed by Zener Holloman parameter equation (parameter Z) [12]:

$$Z = \dot{\varepsilon} \exp\left[\left(\frac{Q}{RT}\right)\right] = A[\sinh(\alpha\sigma)]^n \quad (6)$$

After substituting Eq. 2 and Eq. 3 into Eq. 1, take logarithms on both sides at the same time:

$$ln\dot{\varepsilon} = lnA_1 + n_1 ln\sigma - Q/RT \quad (7)$$

$$ln\dot{\varepsilon} = lnA_2 + \beta\sigma - Q/RT \quad (8)$$

The true stress and true strain data obtained from the experiment when the true strain is 0.3 are substituted into Eq. 4 and Eq. 5. The relationship curves of $ln\dot{\varepsilon} - \sigma$ and $ln\dot{\varepsilon} - ln\sigma$ under different deformation temperatures are drawn by Origin software, as shown in Fig. 3. It can be seen that both $ln\dot{\varepsilon} - \sigma$ and $ln\dot{\varepsilon} - ln\sigma$ have a linear relationship. The slope of different straight lines is obtained by linear fitting of the curve with the least square method. β calculate under higher stress conditions, that is, the average value of the slopes of the two straight lines when the deformation temperature is 300 ℃ and 350 ℃. n_1 is the average value of the slopes of three straight lines when the peak stress is low, that is, the deformation temperature is 400 ℃, 450 ℃ and 500 ℃. Therefore, n_1 = 7.249; α=β/ n_1=0.011.

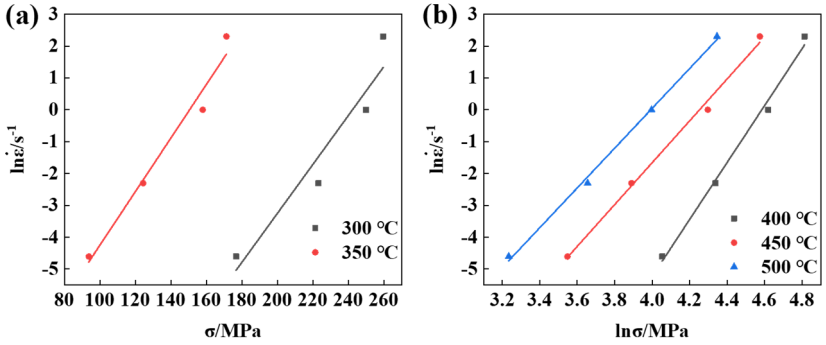

Fig. 4 Relationship curve between $ln\dot{\varepsilon} - \sigma$ and $ln\dot{\varepsilon} - ln\sigma$.

For all stress states, assuming that the activation energy Q is independent of temperature, find the natural logarithm on both sides of Eq. 5:

$$ln\dot{\varepsilon} + \frac{Q}{RT} = lnA + nln[sinh(\alpha\sigma)] \quad (9)$$

The peak stress and the calculated α substitute into Eq. 9 By performing linear regression on the fitting curve in Fig. 4, calculate the average value of different straight-line slopes, and get Q=286.370 $kJ \cdot mol^{-1}$, n = 6.362.

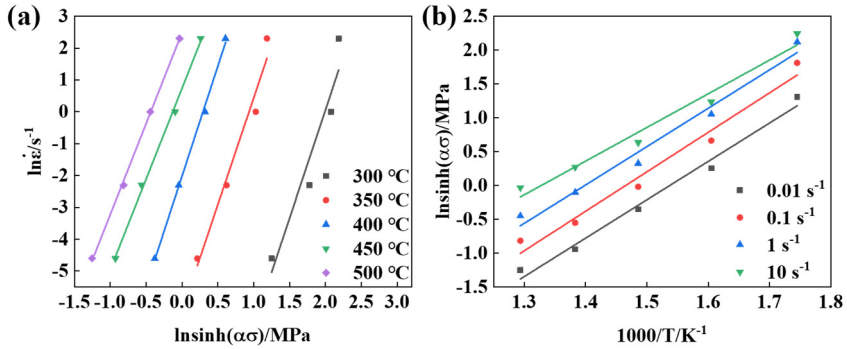

Fig. 5 Relationship curve between $ln[sinh(\alpha\sigma)] - ln\dot{\varepsilon}$ and $ln[sinh(\alpha\sigma)] - T^{-1}$.

Find the natural logarithm on both sides of Eq. 6 at the same time:

$$lnZ = lnA + nln[\sinh(\alpha\sigma)] \quad (10)$$

Fig. 5 shows the relationship curve between ln[sinh (ασ)] and lnZ. A=1.086×1021 s^{-1}can be obtained from its intercept.

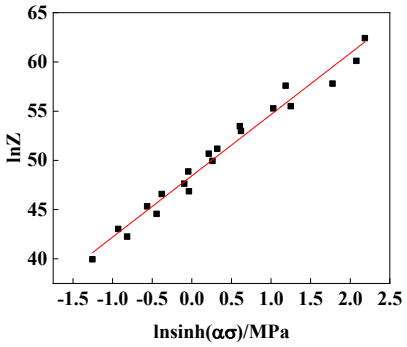

Fig. 6 Relationship curve between lnZ and $ln[\sinh(\alpha\sigma)]$.

Substitute the above calculation data into Eq. 5, and finally obtain the flow stress constitutive model of 2050 aluminum alloy when the real strain is 0.3 as follows:

$$\dot{\varepsilon} = 1.086 \times 10^{21}[\sinh(0.011\sigma)]^{6.362}\, exp(\frac{-286370}{RT}) \quad (11)$$

Select a strain value every 0.05 within the strain range of 0.05 ~ 0.6 for calculation. The calculation steps are the same as above. The material constants of the constitutive model of 2050 aluminum alloy under different strain values can be obtained by substituting the experimental data. The relationship between strain and material constant is established by cubic polynomial fitting. Eq. 12 is a functional relationship.

$$\begin{Bmatrix} \alpha = B_0 + B_1\varepsilon + B_2\varepsilon^2 + B_3\varepsilon^3 + B_4\varepsilon^4 + B_5\varepsilon^5 + B_6\varepsilon^6 \\ n = C_0 + C_1\varepsilon + C_2\varepsilon^2 + C_3\varepsilon^3 + C_4\varepsilon^4 + C_5\varepsilon^5 + C_6\varepsilon^6 \\ Q = D_0 + D_1\varepsilon + D_2\varepsilon^2 + D_3\varepsilon^3 + D_4\varepsilon^4 + D_5\varepsilon^5 + D_6\varepsilon^6 \\ lnA = E_0 + E_1\varepsilon + E_2\varepsilon^2 + E_3\varepsilon^3 + E_4\varepsilon^4 + E_5\varepsilon^5 + E_6\varepsilon^6 \end{Bmatrix} \quad (12)$$

Where B_i, C_i, D_i and $E_i (i = 0,1,2,3,4,5,6)$ are all parameters. Solve the above fitting curve and calculate the parameter values in the formula. Table 2 shows the material constants of 2050 aluminum alloy under different strain conditions.

Table 2 Polynomial function coefficient of material constants (α, n, Q and lnA) about strain.

α		n		Q		lnA	
B_0	0.016	C_0	6.890	D_0	319.793	E_0	51.450
B_1	−0.094	C_1	−6.507	D_1	100.096	E_1	71.909
B_2	0.864	C_2	26.452	D_2	−2165.867	E_2	-871.273
B_3	−4.060	C_3	5.462	D_3	9315.980	E_3	3948.180

B_4	10.005	C_4	−289.438	D_4	−21299.304	E_4	-9463.678
B_5	−12.279	C_5	626.544	D_5	25122.856	E_5	11465.013
B_6	5.914	C_6	−399.280	D_6	−11797.002	E_6	-5477.163

The fitting coefficient and experimental data are substituted into Eq. 5 to obtain the constitutive model of 2050 aluminum alloy. As shown in Fig. 7a, b, c and d, the true stress curve and the predicted value of the constitutive model are shown when the strain rate is 0.01, 0.1, 1 and 10 s^{-1} respectively. It can be seen that the predicted value of the model is close to the true stress curve.

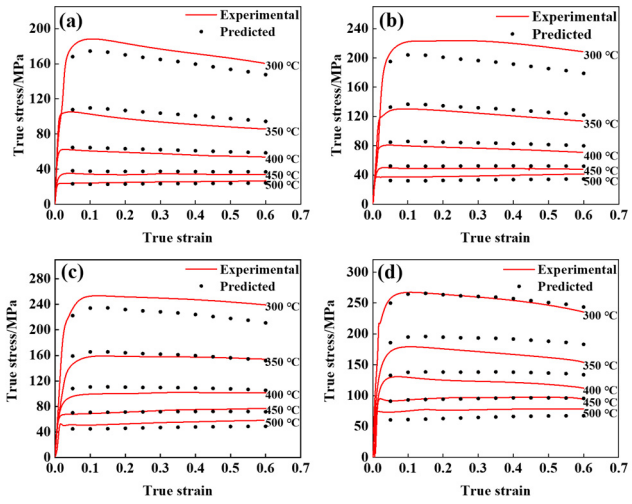

Fig. 7 Experimental and calculated flow stresses at various temperatures and various strain rates: (a)$\dot{\varepsilon} = 0.01s^{-1}$; (b)$\dot{\varepsilon} = 0.1s^{-1}$; (c)$\dot{\varepsilon} = 1s^{-1}$; (d)$\dot{\varepsilon} = 10s^{-1}$

In order to more clearly evaluate the accuracy of 2050 aluminum alloy constitutive model, the following error analysis expression is introduced:

$$R = \frac{\sum_{i=1}^{N}(E_i-\bar{E})(P_i-\bar{P})}{\sqrt{\sum_{i=1}^{N}(E_i-\bar{E})^2 \sum_{i=1}^{N}(P_i-\bar{P})^2}} \quad (13)$$

$$AARE = \frac{1}{N}\sum_{i=1}^{N}\left|\frac{M_i-P_i}{M_i}\right| \quad (14)$$

Where: E is the experimental value of flow stress, P is the predicted value of the model, and N is the number of data groups. Fig. 8 shows the relationship between experimental values and model predicted values. Their correlation coefficient R reaches 0.986 and the average absolute relative error AARE is only 8.59%. It is further verified that the model can accurately predict the true stress of 2050 aluminum alloy under thermal deformation.

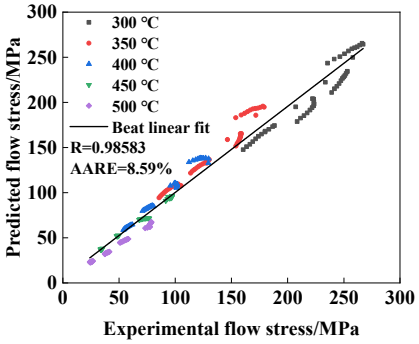

Fig. 8 Comparisons between the experimental and the calculated flow stresses

4. Conclusion

The true stress-strain behavior of 2050 aluminum alloy at 300~500 ℃ and strain rate of 0.01~10 s^{-1} was

studied, and the constitutive model under this deformation parameter was constructed. The conclusions are summarized as follows:

(1) The flow stress enters the steady-state flow stage after the strain strengthening stage, which is related to the recovery and recrystallization softening behavior in the alloy. 2050 aluminum alloy is a positive strain rate sensitive material, and the increase of strain rate leads to the increase of flow stress.

(2) The Arrhenius constitutive model of 2050 aluminum alloy is established. The simulation results obtained by using the established constitutive equation are in good agreement with the experimental results. The correlation coefficient R reached 0.986 and the average absolute relative error AARE is 8.59%.

Acknowledgments

The authors gratefully acknowledgment the Foshan City's Core Technology Research Project (1920001000412) and Defense Industrial Technology Development Program (JCKY2018205B024).

References

[1] Rioja R.J., Liu J. The Evolution of Al-Li Base Products for Aerospace and Space Applications[J]. Metallurgical & Materials Transactions A, 2012, 43(9):3325-3337.

[2] Crill M.J., Chellman D.J., Balmuth E.S., et al. Evaluation of AA 2050-T87 Al-Li Alloy Crack Turning Behaviour[J]. Materials Science Forum, 2006, 519-521:1323-1328.

[3] Wanhill R.J.H, Bray G.H. Aerostructural Design and Its Application to Aluminum–Lithium Alloys[J]. Aluminum-lithium Alloys, 2014, 14(7):27-58.

[4] Li P.W., Li H.Z., L H, et al. Characterization of hot deformation behavior of AA2014 forging aluminum alloy using processing map[J]. Transactions of Nonferrous Metals Society of China, 2017, 27(8):1677-1688.

[5] Dai Q，Liu X，Ping F.U.，et al. High-temperature deformation behavior and processing map of 5083 aluminum alloy[J]. Journal of Central South University (Science and Technology), 2017,48(08):1988-1994 (in Chinese).

[6] Liu N, Xiao D.H., Liu W.S. Microstructure and flow stress behavior of 2055 Al-Li alloy under hot tension[J]. Materials Science and Engineering of Powder Metallurgy, 2020, v.25;No.125(02):39-46 (in Chinese).

[7] Chen Z.Y., Peng W.F., Niu B.K., et al. Hot deformation constitutive equation and hot processing map of 2219 aluminum alloy for super large rings[J]. Journal of Plasticity Engineering, 2020(4):83-92 (in Chinese).

[8] Huang X.D., Zhang H, Han Y, et al. Hot deformation behavior of 2026 aluminum alloy during compression at elevated temperature[J]. Materials Science & Engineering A, 2010, 527(3):485-490.

[9] Bao M, Zhe D.U., Chao L.I., et al. Constitutive behavior and microstructural evolution in hot deformed 2297 Al-Li alloy[J]. Chinese Journal of Aeronautics, 33(4):11.

[10] Gómez G.R., Pérez T. Modelling microstructural development during hot rolling[J]. Materials Science & Technology,1990,6 (11) :1072-1081.

[11] Puchi E.S., Staia M.H. High-temperature deformation of commercial-purity aluminum[J]. Metallurgical & Materials Transactions A,1998,29 (9): 2345-2359.

[12] Zener C, Hollomon J.H. Effect of strain rate upon plastic flow of steel[J]. Journal of Applied Physics,1944,15(1): 22-32.